P10.2 ON THE IMPACT OF VERTICAL RESOLUTION IN THE NUMERICAL FORECASTING OF FOG

Robert Tardif *
National Center for Atmospheric Research, Research Applications Program, Boulder, Colorado

1. INTRODUCTION

In the numerical weather prediction (NWP) literature, numerous studies have aimed at determining the influence of horizontal resolution on the representation of various weather phenomena, such as convection (Weisman et al, 1997), sea-breeze (Colby, 2004), and fog (Pagowski et al., 2004); as well as the overall accuracy of numerical weather forecasts (Mass et al., 2002). Certain weather phenomena have limited vertical extension while still exhibiting distinct features in their vertical structure, such as fog and other boundary layer clouds. This suggests the possible importance of the vertical resolution needed to accurately represent such features, as briefly discussed by Bechtold et al. (1996) for the stratocumulus-topped boundary layer.

In this study, a comprehensive one-dimensional (1D) boundary layer / fog model is used to perform numerical sensitivity experiments aimed at illustrating and gaining insights into the impact of the vertical resolution used to generate explicit short-term forecasts of fog formation and evolution.

2. DESCRIPTION OF MODEL AND EXPERIMENTS

The numerical model used to perform the sensitivity experiment is a modified version of the COBEL (**CO**uche **B**rouillard **E**au **L**iquide) one-dimensional (1D) boundary layer / fog model described in Bergot and Guédalia (1994). The model incorporates comprehensive parameterizations of radiative transfer in the longwave part of the radiation spectrum, a TKE-ℓ turbulent mixing scheme suitable for unstable, neutral, stable and very stable stratification, as well as soil-atmosphere interactions and a bulk microphysical scheme. The original version of the model has been augmented with a comprehensive parameterization of radiative transfer for shortwave (solar) radiation and a module for the evolution of soil moisture and corresponding soil thermal conductivity. Visibility is diagnosed using the translation algorithm proposed by Kunkel (1984) and used in Stoelinga and Warner (1999). Mesoscale factors influencing the state of the local boundary layer, such as the pressure gradient force (geostrophic wind), horizontal advection of temperature and moisture and vertical motion, can be used as input by the 1D model. They can be estimated from careful analysis of data from networks of surface observations or from state-of-the-art 3D mesoscale data assimilation/forecast systems.

* *Corresponding author address*: Robert Tardif, NCAR-RAP, PO Box 3000, Boulder, CO, 80307. E-Mail: tardif@ucar.edu

The original computational grid of the model consists of 30 levels distributed in a log-linear fashion between the surface and a height of 1400 m. Highest vertical resolution is found close to the surface, with grid spacing gradually increasing with height, but remaining less than 30 m in the lowest 200 m of the atmosphere, where fog typically occurs. The evolution of soil temperature and moisture is computed on a grid of 5 levels from a few centimeters below the surface down to a depth of 1 m. The model is integrated with a time step of 30 seconds.

In this paper, COBEL simulations of a well-documented radiation fog event, observed during the Lille 88 field experiment, are performed. Conditions observed from an 80-m tower, soundings and soil sensors, before and during the dense fog event on November 6-7 1988 (Guédalia and Bergot, 1994; referred to as GB94 hereafter), are used to specify the general conditions of the simulations and provide a basis for comparison. Two numerical simulations are performed using different grid configurations. The first configuration corresponds to the original high-resolution (HR) grid used by GB94, while the other configuration has a grid spacing and level placement typical of current operational mesoscale models (referred to as low resolution or LR). Table I shows the heights of computational levels found below 250 m for the two grid configurations.

Table I. Heights (in m) of lower computational levels for the two grid configurations used in the numerical sensitivity experiment.

"High-resolution"	"Low resolution"
0.5	
1.7	
3.1	
4.7	
6.8	
9.3	
12.2	12.2
15.9	
20.2	
25.5	
31.9	31.9
39.6	
49.0	
60.3	
74.0	74.0
90.5	
110.5	
134.7	134.7
164.0	
199.4	
242.2	242.2

All model simulations presented herein are initialized at 1500 UTC (1600 local time) on November 6th, and extend out to 0700 UTC on November 7th. Thus simulations represent short-term (0-16h) fog forecasts. All simulations are initialized using the same profiles, although the structure of initial profiles is somewhat degraded in the reduced resolution experiment, but still captures the main features of the boundary layer (Fig. 1). The initial wind profile is taken from the then operational PERIDOT mesoscale model at Météo-France, in order to preserve a consistency with the specified horizontal pressure force (geostrophic wind). The soil temperature profile down to 1 m is determined using measurements at the tower site, while soil moisture is chosen in order to obtain a soil thermal conductivity of 1.0 W K^{-1} m^{-1} using the relationship proposed by Peters-Lidard et al. (1998).

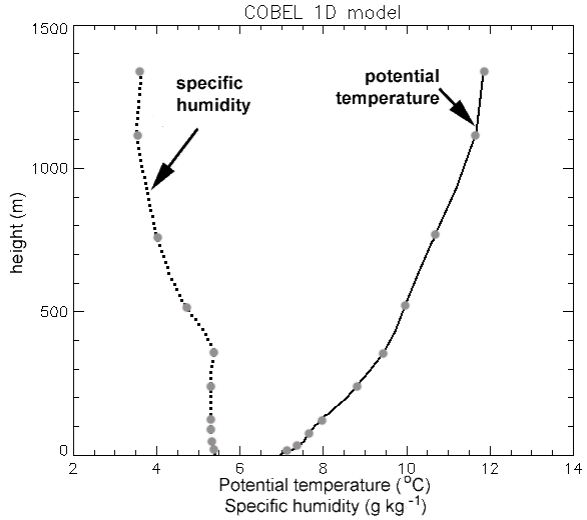

Figure 1. Initial profiles of potential temperature and specific humidity used in the numerical experiments. Profiles were derived from a radiosonde launched at 1500 UTC on November 6th 1988 at the Lille site. Dots represent the data defining the initial profiles of the simulation performed with a low vertical resolution.

The mesoscale forcings are specified using various sources of information such as mesoscale model output and observations from a mesonet and from the tower site. For instance, the evolution of the geostrophic wind profile is derived from the PERIDOT operational forecasts, while horizontal advections are deduced from regional observations. Data from a mesonet suggests the absence of significant low-level temperature advection, while a slight moisture advection is specified in the lowest 250 m between 1800 UTC and 2400 UTC (Fig. 2) in order to obtain a more accurate growth of the fog layer when compared to observations, as in GB94. Also, an additional longwave flux is introduced at the top of the model domain, to reflect the presence of upper level clouds (Fig. 3). Values of this IR flux were determined with the aid of observed downwelling longwave radiation at the top of the Lille tower (GB94).

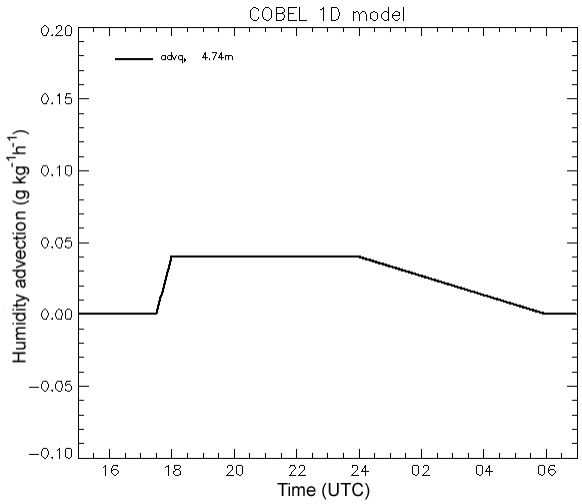

Figure 2. Horizontal advection of moisture introduced in the COBEL 1D simulations of fog for November 6-7 1988 near Lille, northern France.

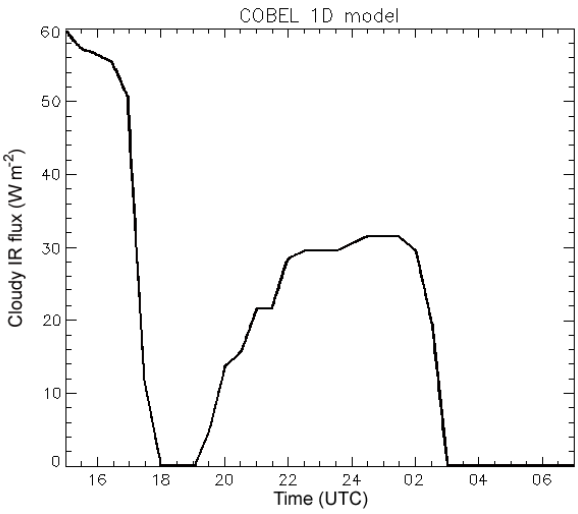

Figure 3. Downwelling longwave flux introduced at the top of the model domain to include radiative effects related to the presence of upper clouds.

3. RESULTS

Results of the numerical experiments performed with the COBEL 1D model are discussed in this section, and diagnostics of model output are examined to provide further insights into the dependence of model behavior on the grid resolution.

3.1 Overall model results

First, the temporal evolution of the near-surface visibility, as predicted by the COBEL model using the two grid configurations, is compared with measurements. Observations at the Lille tower site show a dense fog (visibility below 1000 m) forming at approximately 1800 UTC on the 6th and subsequently

experiencing oscillations until a few minutes after 1900 UTC, at which time a period of heavy fog (visibility below 400 m) begins (Fig. 4). In comparison, the visibility from the HR COBEL run is first reduced below 1000 m close to the surface (1.7 m) at 1700 UTC, while dense fog first appears at 1820 UTC at 4.7 m and just before 2000 UTC at 12.2 m. The initiation of the heavy fog period is about 1 ½ hour too early, although the minimum visibility is reached 1 hour later than observed. For the COBEL run performed with the least number of levels, fog onset at the lowest model level (12.2 m) occurs a few minutes before 2130 UTC, 3 ½ hours later than the initial detection of fog at the site, but about 1 hour too late when compared to visibility observed at a comparable height (Fig. 5b). A general good agreement is observed between the model and observations in terms of the minimum visibility reached near the surface. Nevertheless, a slight tendency for the model to generate a fog that is too dense is observed after 0100 UTC in the two simulations.

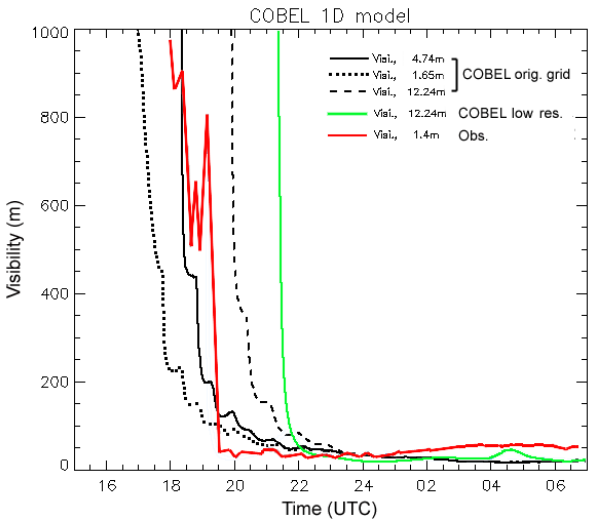

Figure 4. Temporal evolution of visibility: Observed at 1.4 m (red), COBEL using the high-resolution grid at 1.7 m (dotted line), at 4.7 m (solid black line) and at 12.2m (dashed line); and COBEL with a low-resolution grid (lowest model level at 12.2 m) (solid green line).

Taking a look at the vertical growth of the fog layer, Fig. 5 presents time-height contours of cloud water content for the two model simulations. The early stage of the observed growth of the fog layer (until it reached the top of the 80 m tower) is shown by the dots on the figures. It is shown that a shallow ground fog characterized the first two hours of fog development. Starting at 2000 UTC, a rapid growth of the fog layer occurred, reaching 45 m in one hour. A slower upward propagation of the fog is suggested after that, with fog top reaching 80 m after about 6 hours. As discussed in GB94, it is believed that the vertical growth of the fog was influenced by a slight horizontal moisture advection on that particular night. The model run performed with

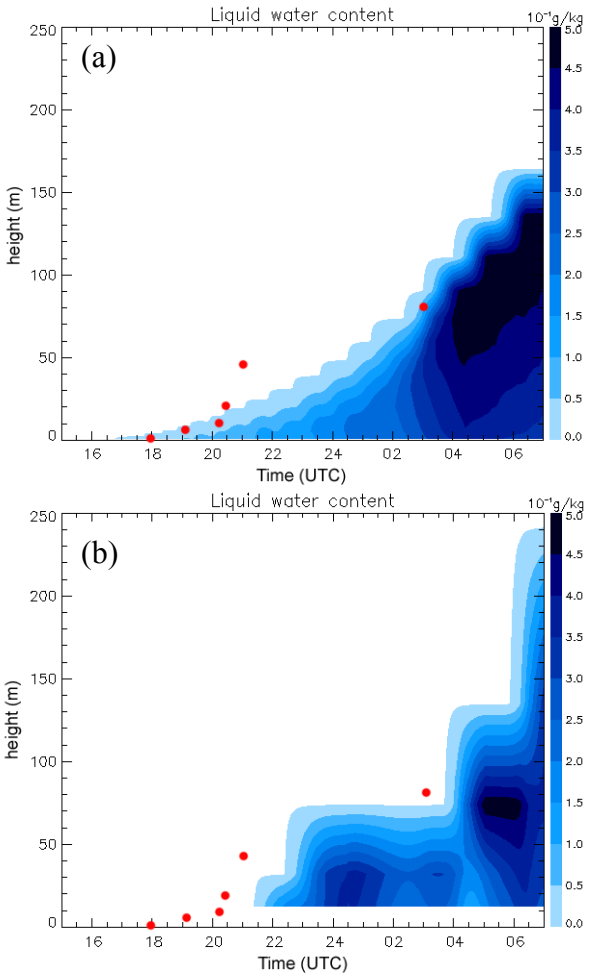

Figure 5. Time-height contour plots of cloud water content simulated with (a) a high-resolution grid, and (b) a grid spacing typical of mesoscale models. Dots indicate the observed time at which fog top reached various heights on the tower.

the high-resolution grid reproduces quite well the "ground fog" stage of the overall evolution of the fog layer, with a gradual increase in fog depth over the first two hours (Fig. 5a). The observed rapid increase in fog depth after 2000 UTC is not accurately represented, as the simulated fog layer shows a more continuous growth. Nevertheless, the observed depth of the fog layer at 0300 UTC is once again very well reproduced by the model. As shown earlier, the run performed with a low resolution is characterized by a fog onset that misses the initial very shallow ground fog. The vertical extension of the simulated fog is too shallow at 0300 UTC with fog water only present up to 32 m (2nd model level). Growth beyond the top of the tower occurs about 1 hour later than observed.

Another noticeable difference between the various model simulations is how the distribution of liquid water content (LWC) evolves in time. For instance, the LWC tends to gradually increase over time and migrate towards fog top after 0200 UTC in the HR simulation (Fig. 5a). The rate of increase of the near-surface LWC

is approximately 0.3 g kg^{-1} h^{-1} until 0200 UTC, and then 0.6 g kg^{-1} h^{-1} over the following 2 hours (Fig. 6). Oscillations are observed, but have relatively small amplitudes. In contrast to this, results obtained from the LR simulation show a tendency to form regions of large LWC in the lower part of the fog early in its evolution, along with large amplitude oscillations. The initial large LWC in the run performed with the lowest vertical resolution occurs after a prolonged and high rate of increase in cloud water, (e.g. 1.2 g kg^{-1} h^{-1} during the first 3 hours of fog). After the initial increase, large amplitude oscillations are observed. Even though such variations in the water content do not translate in large changes in visibility, in this range of water contents at least, the occurrence of such oscillations are not corroborated by the observations (Fig. 4).

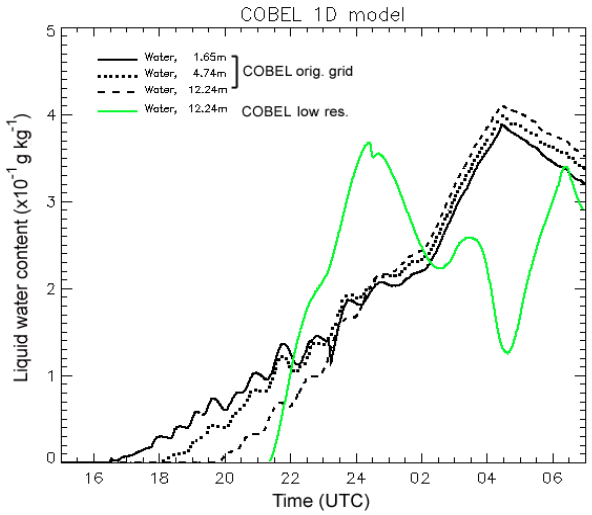

Figure 6. Temporal evolution of cloud water content at the lower model levels for the two simulations performed: COBEL with original grid at 1.7 m (solid line), at 4.7 m (dotted line) and at 12.2m (dashed line); and COBEL with a low resolution grid (lowest model level at 12.2 m) (solid green line).

3.2 Diagnostics

As was shown in the previous section, the LR simulation suffered from deficiencies when compared to observations and to the HR simulation. One of the deficiencies was the delayed formation of fog. Reasons behind this are explored here. First, the evolution of the near-surface temperature is examined (Fig. 7). Observations near the surface show two periods of distinct cooling rates. A cooling rate of 1°C h^{-1} takes place until about 1735 UTC, followed by 2 hours with a cooling rate twice as large. The increase in cooling occurs as upper clouds clear from over the site (Fig. 3). Fog forms during the period of enhanced cooling and becomes denser as cooling continue until 1930 UTC. Then, the temperature increases by several degrees over the next 2 hours. A second minimum is observed just past 0300 UTC, followed by another period of warming during which temperature increases by about 1°C.

The model integrated using the HR grid reproduces well the near-surface cooling observed during the early part of the evening. But, although there is an increase in the cooling after the upper clouds cleared, the model underestimates the subsequent enhanced decrease in temperature (Fig. 7). This is likely the result of the early formation of ground fog in the simulation, thus diminishing the effect of radiative cooling of the surface. For levels located higher, and in particular the one corresponding to the lowest level in the LR run, the cooling rate is generally weaker than closer to the surface. What can be perceived as a paradox is the fog forming earlier in the simulation, even under the influence of weaker cooling than observed. This is most likely related to the evolution of the near-surface moisture. It is probable that the model underestimates the dew deposition at the surface, leading to fog forming somewhat earlier than observed. Unfortunately, reliable observations of humidity are not available, preventing the validation of this hypothesis. After the minimum temperature is reached, along with a LWC of 0.14 g kg^{-1}, a period of warming is simulated as the fog continues its growth. The timing and amplitude of this warming is in error compared to the observations, but still shows the model is able to capture the essence of the dynamics of the foggy boundary layer.

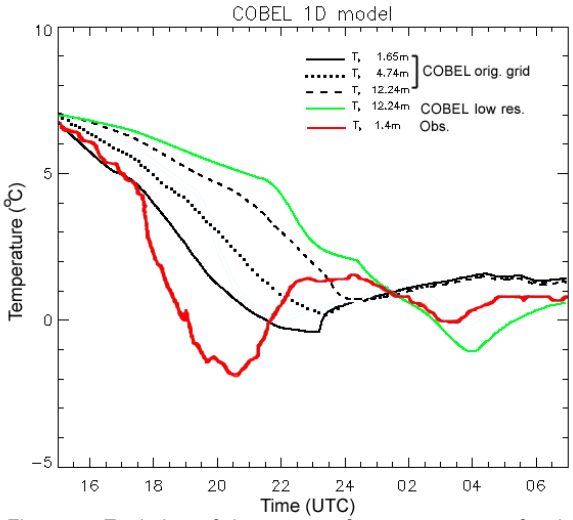

Figure 7. Evolution of the near-surface temperature for the COBEL simulation with the HR grid at 1.7 m (solid line), at 4.7 m (dotted line) and at 12.2m (dashed line); and COBEL with a LR grid (lowest model level at 12.2 m) (solid green line). The observed temperature at 1.4 m is also shown (red line).

Comparing results from the two simulations, the temperature at the lowest model level in the LR run (12 m) exhibits a significantly slower cooling than the temperature at the corresponding height in the HR run. For instance, the 12-m temperature in the HR run is about 0.7°C cooler than in the LR run at 2000 UTC.

Furthermore, cooling continues for much longer, past the time of the initial maximum in LWC in the LR run, with a period of warming only initiated at 0400 UTC.

Now focusing on the early evening near-surface cooling, an examination of the model-diagnosed contributions from radiative and turbulent cooling/heating rates in the surface layer indicate the overall cooling is dominated by the divergence of radiative fluxes for this case. Such a behavior is in agreement with results presented by Ha and Mahrt (2003) for nocturnal boundary layers characterized by light winds, as is the case here. The near-surface profiles of the radiative heating rate calculated using the simulations' initial temperature and moisture profiles are shown in Fig. 8. The lack of resolution of the LR grid close to the surface not only leads to an underestimation of the cooling at the lowest model level (12 m), but also to an inability at capturing the early evening maximum cooling adjacent to the surface. Errors with such a magnitude are in agreement with the study of Räisanen (1996). The heating rates calculated on the LR grid only partially capture the slightly larger cooling in the 10 - 50 m layer, and entirely miss the fine scale structure of the low-level cooling maximum present in the calculated radiative cooling on the HR grid. In contrast, good agreement exists for values found above 60 m. Similar results were obtained throughout the evolution of the early evening boundary layer (not shown).

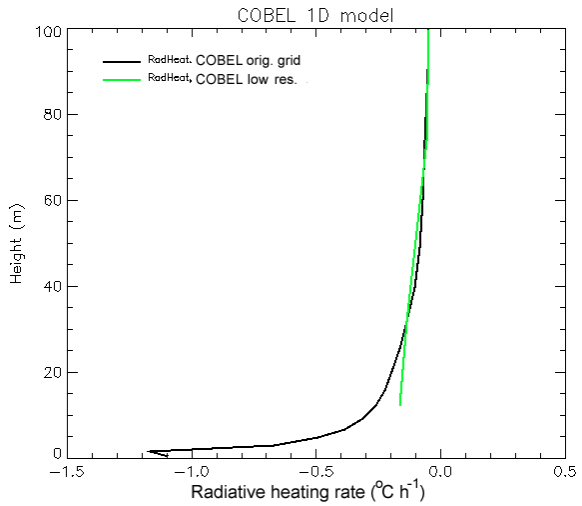

Figure 8. Profiles of radiative heating rates in the lowest 100 m, at 1500 UTC, for the two COBEL simulations: high- (black line) and low- (green line) vertical resolutions.

As was previously pointed out, the temporal evolution of LWC near the surface is quite different between the two COBEL simulations. The LR simulation exhibits a large LWC near the surface which is not present in the HR simulation. The large LWC is the result of a positive feedback between biases in the LWC transport terms and production terms, leading to the significantly larger rate of increase in the LWC seen in Fig. 6. The equation describing the evolution of LWC (q_l) is written as:

$$\frac{\partial q_l}{\partial t} = C + \frac{\partial G}{\partial z} - \frac{\partial \overline{w' q_l'}}{\partial z}, \qquad (1)$$

where q_l is the liquid water mixing ratio, C is the condensation/evaporation of water, G is the sedimentation flux and $\overline{w' q_l'}$ is the turbulent flux of water. The two latter terms can be considered as transport contributions. Within COBEL, the gravitational sedimentation flux is parameterized as

$$G = v_i \cdot q_l, \qquad (2)$$

with v_i (sedimentation velocity) taken as a constant (v_i = 1.6 cm s^{-1}), and the turbulent flux is parameterized as

$$\overline{w' q_l'} = -c \cdot \ell \cdot \sqrt{e} \cdot \frac{\partial q_l}{\partial z}, \qquad (3)$$

where c is a constant, ℓ is a stability dependent mixing length and e is the turbulence kinetic energy. The individual contributions from the transport terms are evaluated from model output at 2148 UTC, a time at which the LWC at 12 m is nearly equal in both simulations (Fig. 6). Results indicate the contributions within the LR simulation are much smaller than compared to the results from the HR simulation. Ratios of contributions from the LR to HR simulations are 48% for the sedimentation and 64% for the turbulent transport terms (see Table II). This shows that condensed water is transported away at a significantly slower rate in the LR simulation than in the HR simulation. The resulting excess water in the LR run then feeds back onto the radiative fluxes, leading to an enhanced radiative cooling rate at fog top, which in turn leads to an even greater production of fog water. This is illustrated in Fig. 8, where a comparison of profiles of the individual contributions to the evolution of potential temperature is shown. Values were estimated at 2224 UTC, 36 minutes after the LWC at 12 m was equal in both simulations. During this time period, the LWC increased in the LR simulation to become about twice as large as in the HR simulation. This time also corresponds to the middle of a period of enhanced cooling in the LR simulation (Fig. 7). It is shown that by that time, the radiative cooling is much larger in the LR model run (70% larger than in the HR run). Also, the turbulent downward mixing of warm air from above leads to a warming that partially counteracts the radiative cooling. Although this contribution is also larger in the LR run, its counteracting effect is not as important as in the HR run. Thus, the combined effects of enhanced radiative cooling and underestimated warming by turbulent fluxes lead to an overall larger cooling rate and a greater production of water. Evidence of this is provided by the larger amount of latent heat

released within the fog layer in the LR run (Fig. 9). This subtle interplay of processes leads to the maximum LWC found near the surface in the LR model simulation.

Table II. Diagnosed contributions to the evolution of fog water content from the divergence of the sedimentation flux and the divergence of the turbulent flux. Estimates are obtained from model output at 2148 UTC in both (high and low resolution) simulations, for the model level at 12.2 m.

Term (g kg^{-1} h^{-1})	"High-resolution"	"Low resolution"
$\frac{\partial G}{\partial z}$	-0.44	-0.21
$\frac{\partial \overline{w' q_l'}}{\partial z}$	-0.0011	-0.0007

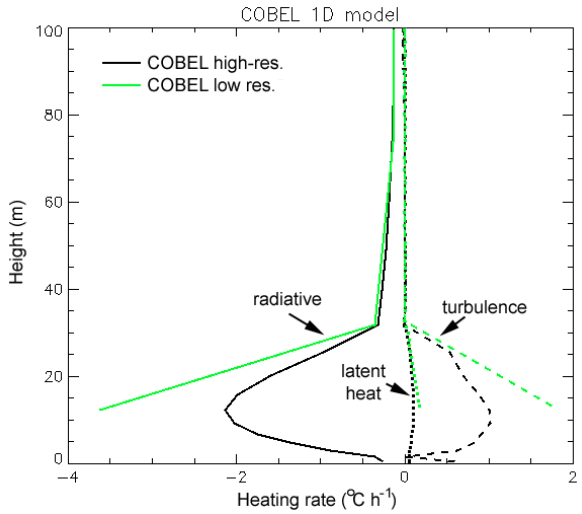

Figure 9. Profiles of contributions to the evolution of potential temperature, diagnosed in the COBEL high-resolution (black) and low-resolution (green) simulations, at 2224 UTC. Contributions are the divergence of net radiation (solid lines), divergence of turbulent heat fluxes (dashed lines) and latent heat (dotted lines).

4. SUMMARY AND CONCLUSIONS

A numerical sensitivity experiment involving the formation and early evolution of a well-documented radiation fog event was performed using the comprehensive COBEL 1D boundary layer / fog model. Model simulations were performed with two different grid configurations, one characterized by a very high-resolution (HR) near the surface and another one with a lower resolution (LR) grid, typical of those used in current mesoscale forecast models. Thus, both simulations were performed with an identical set of physical parameterizations and model numerics. Initial conditions were essentially the same, except for some degradation in resolution of the profiles used for the LR simulation. Mesoscale forcings (geostrophic wind and horizontal moisture advection) were also identical in both models runs.

A comparison of model output from both simulations indicated sensitivity to the vertical resolution. Results from the LR simulation were fairly realistic; however the simulation also showed some deficiencies. In particular, it lacked the desired accuracy in the context of very short-range fog forecasts, as the predicted fog onset occurred noticeably later than observed. A careful examination of model diagnostics suggested that high vertical resolution is required to realistically represent the fine-scale vertical structure and magnitude of the early evening clear-air radiative cooling in the first few meters of the atmosphere, and thus obtain more accurate forecasts of radiation fog onset.

The representation of the overall evolution of the fog layer was also examined. It was found that significant differences in the evolution of the LWC existed between the two simulations. A large maximum in the LWC was generated close to the surface in the LR simulation, while a more gradual increase occurred in the HR simulation. The high rate of increase in LWC resulted from a positive feedback between the underestimation of the transport of LWC and increased radiative cooling.

Given the assumptions and parameterizations used in the COBEL model, it is concluded that the accurate representation of physical processes occurring during the evening transition of the atmospheric boundary layer is of critical importance to the accuracy of very short-term forecasts of fog onset. Results suggest that high vertical resolution is required for the explicit representation of small-scale features found in the clear-sky nocturnal boundary layer as well as in the foggy boundary layer. As such, the profiles of radiative cooling rates and the LWC transport terms were found to be sensitive to the grid resolution. This underlines the need of using high vertical resolution in order to estimate local vertical gradients, found over a few meters only, in order to explicitly represent the mechanisms and interactions determining the evolution of the foggy boundary layer. If high resolution is not possible due to limited computational resources, suitable representations of the subgrid-scale distribution of fog water and associated parameterization of the turbulent flux of water, similar to Bechtold et al. (1992) but adapted to the various stability regimes of the foggy boundary layer should be developed in order to achieve a better performance in the numerical forecasting of fog. The same attention should be put on the parameterization of the sedimentation flux of fog water, as well as on the representation of the radiative effects associated with subgrid-scale features in the clear and cloudy boundary layers.

Acknowledgments

The author would like to thank Dr. Thierry Bergot of CNRM/Météo-France and Dr. Daniel Guédalia of the Laboratoire d'Aérologie, Toulouse, France, for kindly providing the original code of the COBEL model and numerous insights into fog physics and modeling. This research is in response to requirements and funding by the Federal Aviation Administration (FAA). The view expressed are those of the author and do not necessarily represent the official policy of the FAA.

REFERENCES

Bechtold, P., C. Fravalo and J.-P. Pinty, 1992: A model of marine boundary-layer cloudiness for mesoscale applications. *J. Atmos. Sci.*, **49**, 1723-1744.

Bechtold, P., S. K. Krueger, W. S. Lewellen, E. van Meijgaard, C.-H. Moeng, D. A. Randall, A. van Ulden and S. Wang, 1996: "Modeling a stratocumulus-topped PBL: Intercomparison among different one-dimensional codes and with Large Eddy Simulation". *Bull. Amer. Meteor. Soc.*, **77(9)**, 2033-2042.

Bergot, T., and D. Guédalia, 1994: Numerical forecasting of radiation fog. Part I: Numerical model and sensitivity tests. *Mon. Wea. Rev.*, **122**, 1218-1230.

Colby, F. P., 2004: Simulation of the New England sea breeze: The effect of grid spacing. *Wea. Forecasting*, **19**, 277-285.

Guédalia, D. and T. Bergot, 1994: Numerical forecasting of radiation fog. Part II: A comparison of numerical simulation with several observed fog events. *Mon. Wea. Rev.*, **122**, 1231-1246.

Ha, K.-J and L. Mahrt, 2003: Radiative and turbulent fluxes in the nocturnal boundary layer. *Tellus*, **55A**, 317-327.

Kunkel, B. A., 1984: Parameterization of droplet terminal velocity and extinction coefficient in fog models. *J. Climate Appl. Meteor.*, 2**3**, 34-41.

Mass, C. F., D. Ovens, K. Westrick and B. A. Colle, 2002: Does increasing horizontal resolution produce more skillful forecasts? *Bull. Amer. Meteorol. Soc.*, **83**, 407-430.

Pagowski, M., I. Gultepe and P. King, 2004: Analysis and modeling of an extremely dense fog event in southern Ontario. *J. Appl. Meteor.,* **43**, 3-16.

Peters-Lidard, C. D., E. Blackburn, X. Liang and E. F. Wood, 1998: The effect of soil thermal conductivity parameterization on surface energy fluxes and temperatures. *J. Atmos. Sci.*, **55**, 1209-1224.

Räisanen, P., 1996: The effect of vertical resolution on clear-sky radiation calculations: test with two schemes. *Tellus*, **48A**, 403-423.

Stoelinga, M. T. and T. T. Warner, 1999: Nonhydrostatic, mesobeta-scale model simulations of cloud ceiling and visibility for an east-coast winter precipitation event. *J. Appl. Meteor.*, **38**, 385-404.

Weisman, M. L., W. C. Skamarock, and J. B. Klemp, 1997: The resolution dependence of explicitly modeled convective systems. *Mon. Wea. Rev.*, **125**, 527-548.